arXiv:1407.5184v1 [math.NA] 19 Jul 2014

THE FINITE ELEMENT IMMERSED BOUNDARY METHOD WITH DISTRIBUTED LAGRANGE MULTIPLIER

DANIELE BOFFI, NICOLA CAVALLINI, AND LUCIA GASTALDI

ABSTRACT. We introduce a new formulation for the finite element immersed boundary method which makes use of a distributed Lagrange multiplier. We prove that a full discretization of our model, based on a semi-implicit time advancing scheme, is unconditionally stable with respect to the time step size.

1. INTRODUCTION

The Immersed Boundary Method (IBM) is an effective method for the approximation of fluid-structure interaction problems. After its introduction (see [18] and the references therein), which was based on a finite difference approximation of the fluid equations, several attempts have been made in order to consider a finite element version of the IBM; interesting results have been obtained for various formulations (see, in particular [6, 19, 20, 7, 8, 17, 15, 9, 5, 16]). We shall refer to the model introduced in [6] as the FE-IBM formulation.

An important issue when dealing with fluid-structure interactions consists in the choice of the time advancing scheme. For instance, it is well-known that the Arbitrary Lagrangian Eulerian formulation (ALE), which is one of the most popular strategies for dealing with partial differential equations defined on moving domains, suffers from instabilities when approximating biological models (same or similar densities for fluid and solid) unless fully implicit schemes are used for the time evolution. This issue has been explained in [11] with the help of a one dimensional model problem. On the other hand, the FE-IBM method allows for a semi-implicit strategy at the price of a CFL condition which can be more or less severe depending of the fluid and solid dimensions (see [5] for more details).

In the original FE-IBM formulation the evolution of the solid is governed by an ordinary differential equation which reads

$$\frac{\partial \mathbf{X}}{\partial t}(\mathbf{s}, t) = \mathbf{u}(\mathbf{X}(\mathbf{s}, t), t),$$

where $\mathbf{X}$ denotes the position of the solid and $\mathbf{u}$ the fluid velocity (see Problem 1 for more details). In this paper we propose a modification to this approach with the introduction of a suitable Lagrange multiplier. More precisely, the new equation reads

$$\mathbf{c}_1(\boldsymbol{\mu}, \mathbf{u}(\mathbf{X}(\cdot, t), t)) - \mathbf{c}_2\left(\boldsymbol{\mu}, \frac{\partial \mathbf{X}}{\partial t}(\cdot, t)\right) = 0 \qquad \forall \boldsymbol{\mu} \in \Lambda,$$

where $\mathbf{c}_1(\cdot, \cdot)$ and $\mathbf{c}_2(\cdot, \cdot)$ are bilinear forms such that $c_1(\boldsymbol{\mu}, \mathbf{v}(\mathbf{X})) - c_2(\boldsymbol{\mu}, \mathbf{Y}) = 0$ for all $\boldsymbol{\mu} \in \Lambda$ implies $\mathbf{v}(\mathbf{X}) = \mathbf{Y}$.

With this modification, the analogies between the FE-IBM and some versions of the fictitious domain approach become more apparent. In particular, our formulation, which is presented in Problem 2, can be considered as a specific case of a fictitious domain approach with distributed Lagrange multiplier (see [12, 13, 14] for an introduction to this subject). For this reason we shall refer to this new formulation as the DLM-IBM approach. The DLM-IBM share some analogies with a variational formulation presented in [16]. One of the main differences consists in the fact that we are introducing a Lagrange multiplier, thus giving some more flexibility to the resulting numerical scheme.

In this paper we study our new formulation and show that it can be successfully applied to the problem under consideration. More precisely, we prove that a semi-implicit scheme for the time evolution of the DLM-IBM method is unconditionally stable (no restriction at all on the time step). Several numerical examples fully confirm our theoretical findings.

Some additional preliminary studies have been performed in [1, 10], showing that, for some simplified formulation, the DLM-IBM approach is inf-sup stable.

Another important issue for the approximation of incompressible fluids is the discretization of the divergence free constraint on the fluid velocity. This problem is related to the mass conservation properties of the scheme and has been analyzed, in the framework of the FE-IBM, in [3, 4]. Surprisingly enough, it turns out that the DLM-IBM formulation enjoys better mass conservation properties than the original FE-IBM. For the moment, we do not have a theoretical explanation for this phenomenon, which is clearly confirmed by our numerical experiments in Section 6.

The structure of our paper is as follows: in Section 2 we recall the formulation of the FE-IBM, in Section 3 we introduce our DLM-IBM formulation, which is then approximated in time and space in Sections 4 and 5, respectively. Finally, Section 6 reports our numerical experiments.

2. Problem setting

In this section we recall the variational formulation of the IBM for fluid-structure interaction problems presented in [9, 5]. Our formulation covers both the cases of thick and thin structures. In the latter case the region occupied by the structure can be represented as a domain of codimension 1 with respect to the dimension of the fluid region. In the following subsections we introduce the problem corresponding to the two cases.

2.1. **Thick structures.** Let $\Omega \subset \mathbb{R}^d$, $d = 2, 3$, be a bounded domain with Lipschitz continuous boundary. We assume that Ω is subdivided into two connected time dependent subregions Ω_t^f and Ω_t^s, which denote the domains occupied by the fluid and the solid material, respectively. We introduce a Lagrangian framework to deal with the motion of the solid; hence we assume that Ω_t^s can be obtained as the image of a reference domain $\mathcal{B} \subset \mathbb{R}^d$. We denote by $\mathbf{s}$ the position of a point in $\mathcal{B}$ and by $\mathbf{X} : \mathcal{B} \to \Omega_t^s$ the mapping which associates to each $\mathbf{s} \in \mathcal{B}$, the point $\mathbf{x} = \mathbf{X}(\mathbf{s}, t) \in \Omega_t^s$. The deformation gradient is defined as $\mathbb{F} = \boldsymbol{\nabla}_s \mathbf{X}$, the notation $|\mathbb{F}|$ indicates the determinant of the Jacobian matrix $\mathbb{F}$.

The constitutive equations governing the behavior of fluids and solids are the mass balance equation and the conservation of momenta, which in absence of external forces can be written in strong form as follows:

(1)
$$\frac{d\rho}{dt} + \rho \operatorname{div} \mathbf{u} = 0$$
$$\rho \dot{\mathbf{u}} = \rho \frac{D\mathbf{u}}{dt} = \rho \left(\frac{\partial \mathbf{u}}{\partial t} + \mathbf{u} \cdot \boldsymbol{\nabla} \mathbf{u} \right) = \mathbf{div}\, \boldsymbol{\sigma}$$

where $\mathbf{u}$ represents the velocity, $\boldsymbol{\sigma}$ the Cauchy stress-tensor and ρ the mass density.

We assume that both the fluid and the solid material are incompressible. This is equivalent to impose $\operatorname{div} \mathbf{u} = 0$ in Ω. As a consequence, $|\mathbb{F}|$ is constant in time and equals the corresponding value at time $t = 0$. In particular, $|\mathbb{F}| = 1$ if the reference domain coincides with the initial configuration of Ω_t^s, that is $\mathcal{B} = \Omega_0^s$.

Assuming that the fluid and the solid material have mass densities ρ_f and ρ_s, respectively, with $0 < \rho_f \leq \rho_s$, we set

(2)
$$\rho = \left\{ \begin{array}{ll} \rho_f & \text{in } \Omega_t^f \\ \rho_s & \text{in } \Omega_t^s. \end{array} \right.$$

We consider a Newtonian fluid characterized by the usual Navier–Stokes stress tensor

$$\boldsymbol{\sigma}_f = -p\mathbb{I} + \nu \left(\boldsymbol{\nabla} \mathbf{u} + (\boldsymbol{\nabla} \mathbf{u})^\top \right),$$

while the structure is composed by an incompressible viscous hyperelastic material so that the Cauchy stress tensor can be separated into a fluid-like part and an elastic part. Hence we set

(3)
$$\boldsymbol{\sigma} = \left\{ \begin{array}{ll} \boldsymbol{\sigma}_f & \text{in } \Omega_t^f \\ \boldsymbol{\sigma}_f + \boldsymbol{\sigma}_s & \text{in } \Omega_t^s. \end{array} \right.$$

In the following we shall deal with the quantities related to the structure using Lagrangian variables, hence we express the elastic part of the Cauchy stress tensor in term of the first Piola-Kirchhoff stress tensor $\mathbb{P}$ defined as

(4) $$\mathbb{P}(\mathbf{s}, t) = |\mathbb{F}(\mathbf{s}, t)| \boldsymbol{\sigma}_s(\mathbf{x}, t) \mathbb{F}^{-\top}(\mathbf{s}, t) \qquad \text{for } \mathbf{x} = \mathbf{X}(\mathbf{s}, t).$$

From the principle of virtual works, taking into account (2) and (3), we have the following problem in weak form (we refer to [5] for a detailed derivation).

Problem 1. *Given* $\mathbf{u}_0 \in (H_0^1(\Omega))^d$ *and* $\mathbf{X}_0 \in W^{1,\infty}(\mathcal{B})^d$, *find* $(\mathbf{u}(t), p(t)) \in (H_0^1(\Omega))^d \times L_0^2(\Omega)$ *and* $\mathbf{X}(t) \in (H^1(\mathcal{B}))^d$, *such that for almost every* $t \in]0, T[$ *it*

holds

$$\rho_f \frac{d}{dt}(\mathbf{u}(t), \mathbf{v}) + b(\mathbf{u}(t), \mathbf{u}(t), \mathbf{v}) + a(\mathbf{u}(t), \mathbf{v})$$

$$\text{(5a)} \qquad - (\operatorname{div} \mathbf{v}, p(t)) = \langle \mathbf{d}(t), \mathbf{v} \rangle + \langle \mathbf{F}(t), \mathbf{v} \rangle \qquad \forall \mathbf{v} \in (H_0^1(\Omega))^d$$

$$\text{(5b)} \qquad (\operatorname{div} \mathbf{u}(t), q) = 0 \qquad \forall q \in L_0^2(\Omega)$$

$$\text{(5c)} \qquad \langle \mathbf{d}(t), \mathbf{v} \rangle = -\delta\rho \int_{\mathcal{B}} \frac{\partial^2 \mathbf{X}}{\partial t^2} \mathbf{v}(\mathbf{X}(\mathbf{s}, t)) \, d\mathbf{s} \qquad \forall \mathbf{v} \in (H_0^1(\Omega))^d$$

$$\text{(5d)} \qquad \langle \mathbf{F}(t), \mathbf{v} \rangle = -\int_{\mathcal{B}} \mathbb{P}(\mathbb{F}(\mathbf{s}, t)) : \nabla_s \mathbf{v}(\mathbf{X}(\mathbf{s}, t)) \, d\mathbf{s} \qquad \forall \mathbf{v} \in (H_0^1(\Omega))^d$$

$$\text{(5e)} \qquad \frac{\partial \mathbf{X}}{\partial t}(\mathbf{s}, t) = \mathbf{u}(\mathbf{X}(\mathbf{s}, t), t) \qquad \forall \mathbf{s} \in \mathcal{B}$$

$$\text{(5f)} \qquad \mathbf{u}(0) = \mathbf{u}_0 \quad \text{in } \Omega, \qquad \mathbf{X}(0) = \mathbf{X}_0 \quad \text{in } \mathcal{B}.$$

Here $\delta\rho = \rho_s - \rho_f$, $(\cdot, \cdot)$ stands for the scalar product in $L^2(\Omega)$, $\mathbb{D} : \mathbb{E} = \sum_{\alpha, i=1}^{d} \mathbb{D}_{\alpha i} \mathbb{E}_{\alpha i}$ for all tensors $\mathbb{D}$ and $\mathbb{E}$ and

$$a(\mathbf{u}, \mathbf{v}) = \boldsymbol{\mu}(\boldsymbol{\nabla}_{\text{sym}} \mathbf{u}, \boldsymbol{\nabla}_{\text{sym}} \mathbf{v}) \quad \text{with } \boldsymbol{\nabla}_{\text{sym}} \mathbf{u} = \boldsymbol{\nabla} \mathbf{u} + (\boldsymbol{\nabla} \mathbf{u})^\top,$$

$$b(\mathbf{u}, \mathbf{v}, \mathbf{w}) = \frac{\rho_f}{2}((\mathbf{u} \cdot \boldsymbol{\nabla} \mathbf{v}, \mathbf{w}) - (\mathbf{u} \cdot \boldsymbol{\nabla} \mathbf{w}, \mathbf{v})).$$

2.2. **Thin structures.** Let us now consider the case of a thin structure with constant thickness t_s very small. Therefore we can assume that the physical quantities depend only on variables along the middle section of the structure and are constant in the orthogonal direction and we consider mathematically the region occupied by the structure as a curve immersed in a two dimensional fluid or a surface in a three dimensional one. Hence we have that $\Omega_t^s \subset \mathbb{R}^d$, $\mathcal{B} \subset \mathbb{R}^m$ with $m = d - 1$, $\mathbf{X} : \mathcal{B} \to \Omega$ and the deformation gradient $\mathbb{F} : \mathcal{B} \to \mathbb{R}^{d \times m}$ is such that

$$|\mathbb{F}| = \left| \frac{\partial \mathbf{X}}{\partial s} \right| \text{ if } m = 1, \qquad |\mathbb{F}| = \left| \frac{\partial \mathbf{X}}{\partial s_1} \times \frac{\partial \mathbf{X}}{\partial s_2} \right| \text{ if } m = 2,$$

s, s_1 and s_2 being the parametric variables in $\mathcal{B}$.

In [5] we have shown that the variational formulation of the fluid-structure interaction problem has the same form as Problem 1 if we set $\delta\rho = (\rho_s - \rho_f)t_s$ and $\mathbb{P} = t_s \tilde{\mathbb{P}}$ where $\tilde{\mathbb{P}}$ is obtained with the due modifications from (4). Notice that $\mathbb{P}$ is a tensor with the same dimensions as $\mathbb{F}$.

2.3. **Stability estimate.** We end this section by recalling an energy estimate which follows from the assumptions on the elastic properties of hyperelastic material which we are considering in this paper. The results of this section can be found in more detail in [15, 9, 5]. The hyperelastic materials are characterized by a positive energy density $W(\mathbb{F})$ which depends only on the deformation gradient. The energy density is related to the first Piola–Kirchhoff stress tensor by means of the following relation:

$$\text{(6)} \qquad (\mathbb{P}(\mathbb{F}(\mathbf{s}, t))_{\alpha i} = \frac{\partial W}{\partial \mathbb{F}_{\alpha i}}(\mathbb{F}(\mathbf{s}, t)) = \left(\frac{\partial W}{\partial \mathbb{F}}(\mathbb{F}(\mathbf{s}, t)) \right)_{\alpha i},$$

where $i = 1, \dots, m$ and $\alpha = 1, \dots, d$.

At the end, the elastic potential energy of the body is given by:

$$(7) \qquad E\left(\mathbf{X}(t)\right) = \int_{\mathcal{B}} W(\mathbb{F}(s,t))\mathrm{d}\mathbf{s}.$$

We make the following assumption on the potential energy density W which will be useful in the following sections.

Assumption 1. *We assume that W is a C^1 convex function over the set of second order tensors.*

Remark. Even though in general elasticity problems the potential energy should assumed polyconvex, Assumption 1 makes sense in this context since our material is incompressible, so that $|\mathbb{F}|$ is constant in time.

In the following proposition, we recall the stability estimate proved in [5].

Proposition 1. *Let us assume that for almost every $t \in [0,T]$, $\mathbf{u}(t) \in (H_0^1(\Omega))^d$ and $\mathbf{X}(t) \in (W^{1,\infty}(\mathcal{B}))^d$ solve Problem 1, then the following bound holds true*

$$(8) \qquad \frac{\rho_f}{2}\frac{d}{dt}||\mathbf{u}(t)||_0^2 + \nu||\,\boldsymbol{\nabla}_{\mathrm{sym}}\,\mathbf{u}(t)||_0^2 + \frac{\delta\rho}{2}\frac{d}{dt}\left\|\frac{\partial\mathbf{X}}{\partial t}\right\|_{0,\mathcal{B}}^2 + \frac{d}{dt}E(\mathbf{X}(t)) = 0,$$

where $\|\cdot\|_0$ and $\|\cdot\|_{0,\mathcal{B}}$ denote the norms in $L^2(\Omega)$ and $L^2(\mathcal{B})$, respectively.

The above a priori estimate states that a solution of Problem 1, if exists, enjoys the following regularity properties

$$\mathbf{u} \in C^0([0,T];(H_0^1(\Omega))^d) \cap H^1(0,T;(L^2(\Omega))^d)$$
$$p \in L^2(0,T;H^1(\Omega))$$
$$\mathbf{X} \in W^{1,\infty}(0,T;L^2(\mathcal{B})^d)$$
$$E\left(\mathbf{X}(t)\right) \in L^\infty(0,T).$$

3. Fictitious domain formulation with distributed Lagrange multiplier

Proposition 1 is fundamental in the treatment of the numerical approximation of the problem; in particular, one would like to have the same property for the discrete version of Problem 1. However, it was shown in previous papers on the finite element discretization of the problem that the space semi-discrete version of Problem 1 enjoys the same stability properties, while the time-space discretization requires a CFL condition which limits the time step in terms of the size of the meshes unless a fully implicit formulation is considered (see [8, 7, 15, 5]). Here we present a new formulation of Problem 1 based on the introduction of a Lagrange multiplier to enforce the motion condition (5e) which turns out to be unconditionally stable after time discretization. We present separately such formulation for the case of structures of codimension zero and one.

We consider three functional spaces Λ, M_1 and M_2, and two bilinear forms $\mathbf{c}_1 : \Lambda \times M_1 \to \mathbb{R}$ and $\mathbf{c}_2 : \Lambda \times M_2 \to \mathbb{R}$ such that the equation

$$\mathbf{c}_1(\boldsymbol{\mu},\mathbf{v}(\overline{\mathbf{X}})) - \mathbf{c}_2(\boldsymbol{\mu},\mathbf{Y}) = 0 \quad \forall\boldsymbol{\mu} \in \Lambda$$

implies that $\mathbf{v}(\overline{\mathbf{X}}) = \mathbf{Y}$ for a given $\overline{\mathbf{X}} \in W^{1,\infty}(\mathcal{B})$.

3.1. **Thick structures.** Let us set $m = d$ and assume that for almost every $t \in\ ]0, T[$ we have that $\mathbf{X}(t) \in W^{1,\infty}(\mathcal{B})^d$, so that $\mathbf{u}(\mathbf{X}(\cdot, t), t) \in (H^1(\mathcal{B}))^d$.

In this case, we set $M_1 = (H_0^1(\Omega))^d$, $M_2 = (H^1(\mathcal{B}))^d$ and we consider two possible choices for the bilinear forms $\mathbf{c}_1$, $\mathbf{c}_2$ and the space Λ. The most natural one is to let Λ be the dual space of $(H^1(\mathcal{B}))^d$, that is $\Lambda = ((H^1(\mathcal{B}))^d)'$, then $\mathbf{c}_2$ is given by the duality pairing between $((H^1(\mathcal{B}))^d)'$ and $(H^1(\mathcal{B}))^d$, and $\mathbf{c}_1$ is defined accordingly for a given $\mathbf{X} \in W^{1,\infty}(\mathcal{B})^d$, namely

$$(9) \quad \begin{aligned} \mathbf{c}_1(\boldsymbol{\lambda}, \mathbf{v}(\mathbf{X})) &= \langle \boldsymbol{\lambda}, \mathbf{v}(\mathbf{X}) \rangle & \boldsymbol{\lambda} \in \Lambda = ((H^1(\mathcal{B}))^d)', \ \mathbf{v} \in (H_0^1(\Omega))^d \\ \mathbf{c}_2(\boldsymbol{\lambda}, \mathbf{Y}) &= \langle \boldsymbol{\lambda}, \mathbf{Y} \rangle & \boldsymbol{\lambda} \in \Lambda = ((H^1(\mathcal{B}))^d)', \ \mathbf{Y} \in (H^1(\mathcal{B}))^d. \end{aligned}$$

Alternatively, we can associate to any $\boldsymbol{\lambda} \in ((H^1(\mathcal{B}))^d)'$ an element $\boldsymbol{\varphi} \in (H^1(\mathcal{B}))^d$ solution to the following variational equation:

$$(10) \qquad \int_{\mathcal{B}} (\boldsymbol{\nabla}_s \boldsymbol{\varphi} \cdot \boldsymbol{\nabla}_s \mathbf{Y} + \boldsymbol{\varphi} \cdot \mathbf{Y}) \, d\mathbf{s} = \langle \boldsymbol{\lambda}, \mathbf{Y} \rangle, \quad \forall \mathbf{Y} \in (H^1(\mathcal{B}))^d.$$

We observe that the integral on the left hand side is the scalar product in $(H^1(\mathcal{B}))^d$ and that it is easy to show that there exists a unique $\boldsymbol{\varphi} \in (H^1(\mathcal{B}))^d$ satisfying (10) with the following relation

$$\|\boldsymbol{\varphi}\|_{(H^1(\mathcal{B}))^d} = \|\boldsymbol{\lambda}\|_{((H^1(\mathcal{B}))^d)'}.$$

Hence we can also define $\mathbf{c}_1$ and $\mathbf{c}_2$ as follows. We set $\Lambda = (H^1(\mathcal{B}))^d$, and
(11)

$$\mathbf{c}_1(\boldsymbol{\lambda}, \mathbf{v}(\mathbf{X})) = \int_{\mathcal{B}} (\boldsymbol{\nabla}_s \boldsymbol{\lambda} \cdot \boldsymbol{\nabla}_s \mathbf{v}(\mathbf{X}) + \boldsymbol{\lambda} \cdot \mathbf{v}(\mathbf{X})) \, d\mathbf{s} \qquad \boldsymbol{\lambda} \in \Lambda, \ \mathbf{v} \in (H_0^1(\Omega))^d$$

$$\mathbf{c}_2(\boldsymbol{\lambda}, \mathbf{Y}) = \int_{\mathcal{B}} (\boldsymbol{\nabla}_s \boldsymbol{\lambda} \cdot \boldsymbol{\nabla}_s \mathbf{Y} + \boldsymbol{\lambda} \cdot \mathbf{Y}) \, d\mathbf{s} \qquad \boldsymbol{\lambda} \in \Lambda = (H^1(\mathcal{B}))^d, \ \mathbf{Y} \in (H^1(\mathcal{B}))^d.$$

Using either definition (9) or (11), equation (5e) can be written variationally as

$$(12) \qquad \mathbf{c}_1(\boldsymbol{\mu}, \mathbf{u}(\mathbf{X}(\cdot, t), t)) - \mathbf{c}_2\left(\boldsymbol{\mu}, \frac{\partial \mathbf{X}}{\partial t}(t)\right) = 0 \quad \forall \boldsymbol{\mu} \in \Lambda.$$

Let us introduce a Lagrange multiplier $\boldsymbol{\lambda}(t) \in \Lambda$ associated to the constraint (12) and split equation (5a) as follows:
(13)

$$\rho_f \frac{d}{dt}(\mathbf{u}(t), \mathbf{v}) + b(\mathbf{u}(t), \mathbf{u}(t), \mathbf{v}) + a(\mathbf{u}(t), \mathbf{v}) + \mathbf{c}_1(\boldsymbol{\lambda}(t), \mathbf{v}(\mathbf{X}(t))) = 0 \quad \forall \mathbf{v} \in (H_0^1(\Omega))^d$$

$$\delta\rho \left(\frac{\partial^2 \mathbf{X}}{\partial t^2}(t), \mathbf{Y}\right)_{\mathcal{B}} + (\mathbb{P}(\mathbb{F}(t)), \boldsymbol{\nabla}_s \mathbf{Y})_{\mathcal{B}} - \mathbf{c}_2(\boldsymbol{\lambda}(t), \mathbf{Y}) = 0 \qquad \forall \mathbf{Y} \in (H^1(\mathcal{B}))^d,$$

where we have denoted by $(\cdot, \cdot)_{\mathcal{B}}$ the scalar product in $L^2(\mathcal{B})^d$. Then Problem 1 can be written as follows.

Problem 2. *Given* $\mathbf{u}_0 \in (H_0^1(\Omega))^d$ *and* $\mathbf{X}_0 \in W^{1,\infty}(\mathcal{B})$, *find* $(\mathbf{u}(t), p(t)) \in (H_0^1(\Omega))^d \times L_0^2(\Omega)$, $\mathbf{X}(t) \in (H^1(\mathcal{B}))^d$, *and* $\boldsymbol{\lambda}(t) \in \Lambda$, *such that for almost every* $t \in\ ]0, T[$ *it holds*

$$\rho_f \frac{d}{dt}(\mathbf{u}(t), \mathbf{v}) + b(\mathbf{u}(t), \mathbf{u}(t), \mathbf{v}) + a(\mathbf{u}(t), \mathbf{v})$$

(14a) $\qquad - (\operatorname{div} \mathbf{v}, p(t)) + \mathbf{c}_1(\boldsymbol{\lambda}(t), \mathbf{v}(\mathbf{X}(t))) = 0 \qquad\qquad \forall \mathbf{v} \in (H_0^1(\Omega))^d$

(14b) $(\operatorname{div} \mathbf{u}(t), q) = 0 \qquad\qquad\qquad\qquad\qquad \forall q \in L_0^2(\Omega)$

(14c) $\delta\rho \left(\dfrac{\partial^2 \mathbf{X}}{\partial t^2}(t), \mathbf{Y} \right)_{\mathcal{B}} + (\mathbb{P}(\mathbb{F}(t)), \boldsymbol{\nabla}_s \mathbf{Y})_{\mathcal{B}} - \mathbf{c}_2(\boldsymbol{\lambda}(t), \mathbf{Y}) = 0 \quad \forall \mathbf{Y} \in (H^1(\mathcal{B}))^d$

(14d) $\mathbf{c}_1(\boldsymbol{\mu}, \mathbf{u}(\mathbf{X}(\cdot, t), t)) - \mathbf{c}_2 \left(\boldsymbol{\mu}, \dfrac{\partial \mathbf{X}}{\partial t}(t) \right) = 0 \qquad\qquad \forall \boldsymbol{\mu} \in \Lambda$

(14e) $\mathbf{u}(0) = \mathbf{u}_0 \quad \text{in } \Omega, \qquad \mathbf{X}(0) = \mathbf{X}_0 \quad \text{in } \mathcal{B}.$

It is easy to check that Problems 1 and 2 are equivalent if $\mathbf{X}(t) \in (W^{1,\infty}(\mathcal{B}))^d$. Moreover, we have the following energy estimate.

Proposition 2. *For almost every* $t \in]0, T[$, *let* $\mathbf{u}(t) \in (H_0^1(\Omega))^d$ *and* $\mathbf{X}(t) \in (H^1(\mathcal{B}))^d$ *be solution of Problem 2 with* $\partial \mathbf{X}(t)/\partial t \in (L^2(\mathcal{B}))^d$ *then the following energy estimate holds true*

(15) $\qquad \dfrac{\rho_f}{2} \dfrac{d}{dt} \|\mathbf{u}(t)\|_0^2 + \nu \|\nabla \mathbf{u}(t)\|_0^2 + \dfrac{\delta\rho}{2} \dfrac{d}{dt} \left\| \dfrac{\partial \mathbf{X}}{\partial t} \right\|_{0,\mathcal{B}}^2 + \dfrac{d}{dt} E(\mathbf{X}(t)) = 0.$

Proof. Taking $\mathbf{v} = \mathbf{u}(t)$ in (14a) and $q = p(t)$ in (14b), and recalling that $b(\mathbf{u}, \mathbf{u}, \mathbf{u}) = 0$ by definition, we get

$$\dfrac{\rho_f}{2} \dfrac{d}{dt} \|\mathbf{u}(t)\|_0^2 + \nu \|\boldsymbol{\nabla}_{\text{sym}} \mathbf{u}\|_0^2 + \mathbf{c}_1(\boldsymbol{\lambda}(t), \mathbf{u}(\mathbf{X}(\cdot, t), t)) = 0.$$

Next we consider (14c) and take $\mathbf{Y} = \partial \mathbf{X}(t)/\partial t$, obtaining

$$\dfrac{\delta\rho}{2} \dfrac{d}{dt} \left\| \dfrac{\partial \mathbf{X}}{\partial t}(t) \right\|_{0,\mathcal{B}}^2 + \left(\mathbb{P}(\mathbb{F}(t)), \boldsymbol{\nabla}_s \left(\dfrac{\partial \mathbf{X}}{\partial t}(t) \right) \right)_{\mathcal{B}} - \mathbf{c}_2 \left(\boldsymbol{\lambda}(t), \dfrac{\partial \mathbf{X}}{\partial t}(t) \right) = 0.$$

Recalling the definition of the energy density and of the elastic potential energy (6)-(7), we have

$$\left(\mathbb{P}(\mathbb{F}(t)), \boldsymbol{\nabla}_s \left(\dfrac{\partial \mathbf{X}}{\partial t}(t) \right) \right)_{\mathcal{B}} = \int_{\mathcal{B}} \dfrac{\partial W}{\partial \mathbf{F}}(\mathbf{F}(\mathbf{s}, t)) \dfrac{\partial}{\partial t} \boldsymbol{\nabla}_s \mathbf{X}(\mathbf{s}, t) \mathrm{d}\mathbf{s}$$

$$= \int_{\mathcal{B}} \dfrac{\partial W}{\partial \mathbf{F}}(\mathbf{F}(\mathbf{s}, t)) \dfrac{\partial \mathbf{F}}{\partial t}(\mathbf{s}, t) \mathrm{d}\mathbf{s}$$

$$= \dfrac{d}{dt} \int_{\mathcal{B}} W(\mathbf{F}(\mathbf{s}, t)) \mathrm{d}\mathbf{s} = \dfrac{d}{dt} (E(\mathbf{X}(t))).$$

Combining the last equations and taking into account (14d) we arrive at (15). $\qquad \square$

3.2. **Thin structures.** Let us now set $m = d-1$; we observe that equation (5e) has to be intended in the sense of traces of functions in $(H_0^1(\Omega))^d$. Assuming that, for a.e. $t \in]0, T[$, $\mathbf{X}(t) \in (W^{1,\infty}(\mathcal{B}))^d$, the trace of $\mathbf{u}(t)$ along $\mathcal{B}_t$ belongs to $(H^{1/2}(\mathcal{B}_t))^d$ or equivalently $\mathbf{u}(\mathbf{X}(\cdot, t), t) \in (H^{1/2}(\mathcal{B}))^d$. Hence we can set $M_1 = (H_0^1(\Omega))^d$, $M_2 = (H^1(\mathcal{B}))^d$, and $\Lambda = (H^{1/2}(\mathcal{B})^d)'$. Then a natural definition for the forms $\mathbf{c}_1$ and $\mathbf{c}_2$ can be

$$\mathbf{c}_1(\boldsymbol{\lambda}, \mathbf{v}(\mathbf{X})) = \langle \boldsymbol{\lambda}, \mathbf{v}(\mathbf{X}) \rangle \qquad \boldsymbol{\lambda} \in \Lambda, \ \mathbf{v} \in (H_0^1(\Omega))^d$$

$$\mathbf{c}_2(\boldsymbol{\lambda}, \mathbf{Y}) = \langle \boldsymbol{\lambda}, \mathbf{Y} \rangle \qquad \boldsymbol{\lambda} \in \Lambda, \ \mathbf{Y} \in (H^1(\mathcal{B}))^d.$$

Then working as in the previous subsection we can write Problem 1 in the equivalent form given by Problem 2 provided we use the correct bilinear forms $\mathbf{c}_1$ and $\mathbf{c}_2$. Proposition 2 holds true without any modifications.

4. Time advancing scheme

In this section we introduce a semi-discretization in time of Problem 2. Let us subdivide the time interval $[0, T]$ into N equal parts and let Δt be the corresponding time step. For $n = 0, \ldots, N$ let $t_n = n\Delta t$; by the superscript n we indicate the value of an unknown function at time t_n. Then a fully implicit scheme reads: given $\mathbf{u}_0 \in (H_0^1(\Omega))^d$ and $\mathbf{X}_0 \in W^{1,\infty}(\mathcal{B})$, for $n = 1, \ldots, N$ find $(\mathbf{u}^n, p^n) \in (H_0^1(\Omega))^d \times L_0^2(\Omega)$, $\mathbf{X}^n \in (H^1(\mathcal{B}))^d$, and $\boldsymbol{\lambda}^n \in \Lambda$, such that

$$\rho_f \left(\frac{\mathbf{u}^{n+1} - \mathbf{u}^n}{\Delta t}, \mathbf{v} \right) + b(\mathbf{u}^{n+1}, \mathbf{u}^{n+1}, v) + a(\mathbf{u}^{n+1}, \mathbf{v})$$
$$- (\operatorname{div} \mathbf{v}, p^{n+1}) + \mathbf{c}_1(\boldsymbol{\lambda}^{n+1}, v(\mathbf{X}^{n+1})) = 0 \quad \forall \mathbf{v} \in (H_0^1(\Omega))^d$$
$$(\operatorname{div} \mathbf{u}^{n+1}, q) = 0 \quad \forall q \in L_0^2(\Omega)$$
$$\delta\rho \left(\frac{\mathbf{X}^{n+1} - 2\mathbf{X}^n + \mathbf{X}^{n-1}}{\Delta t^2}, \mathbf{Y} \right)_{\mathcal{B}} + (\mathbb{P}(\mathbb{F}^{n+1}), \boldsymbol{\nabla}_s \mathbf{Y})_{\mathcal{B}}$$
$$- \mathbf{c}_2(\boldsymbol{\lambda}^{n+1}, \mathbf{Y}) = 0 \quad \forall \mathbf{Y} \in (H^1(\mathcal{B}))^d$$
$$\mathbf{c}_1(\boldsymbol{\mu}, \mathbf{u}^{n+1}(\mathbf{X}^{n+1})) - \mathbf{c}_2 \left(\boldsymbol{\mu}, \frac{\mathbf{X}^{n+1} - \mathbf{X}^n}{\Delta t} \right) = 0 \quad \forall \boldsymbol{\mu} \in \Lambda.$$

The main trouble in the above system consists in the computation of the terms involving functions belonging to $H_0^1(\Omega)$ evaluated along the structure through the mapping $\mathbf{X}^{n+1}$. We then choose to evaluate these terms using the mapping at the previous time step. Analogously, the convective term is linearized by computing the transport velocity at the previous step. The scheme is then modified as follows.

Problem 3. *Given $\mathbf{u}_0 \in (H_0^1(\Omega))^d$ and $\mathbf{X}_0 \in W^{1,\infty}(\mathcal{B})$, for $n = 1, \ldots, N$ find $(\mathbf{u}^n, p^n) \in (H_0^1(\Omega))^d \times L_0^2(\Omega)$, $\mathbf{X}^n \in (H^1(\mathcal{B}))^d$, and $\boldsymbol{\lambda}^n \in ((H^1(\mathcal{B}))^d)'$, such that*

$$\rho_f \left(\frac{\mathbf{u}^{n+1} - \mathbf{u}^n}{\Delta t}, \mathbf{v} \right) + b(\mathbf{u}^n, \mathbf{u}^{n+1}, v) + a(\mathbf{u}^{n+1}, \mathbf{v})$$
(16a)
$$- (\operatorname{div} \mathbf{v}, p^{n+1}) + \mathbf{c}_1(\boldsymbol{\lambda}^{n+1}, v(\mathbf{X}^n)) = 0 \,\forall \mathbf{v} \in (H_0^1(\Omega))^d$$

(16b) $(\operatorname{div} \mathbf{u}^{n+1}, q) = 0 \qquad \forall q \in L_0^2(\Omega)$

$$\delta\rho \left(\frac{\mathbf{X}^{n+1} - 2\mathbf{X}^n + \mathbf{X}^{n-1}}{\Delta t^2}, \mathbf{Y} \right)_{\mathcal{B}} + (\mathbb{P}(\mathbb{F}^{n+1}), \boldsymbol{\nabla}_s \mathbf{Y})_{\mathcal{B}}$$
(16c)
$$- \mathbf{c}_2(\boldsymbol{\lambda}^{n+1}, \mathbf{Y}) = 0 \qquad \forall \mathbf{Y} \in (H^1(\mathcal{B}))^d$$

(16d) $\mathbf{c}_1(\boldsymbol{\mu}, \mathbf{u}^{n+1}(\mathbf{X}^n)) - \mathbf{c}_2 \left(\boldsymbol{\mu}, \frac{\mathbf{X}^{n+1} - \mathbf{X}^n}{\Delta t} \right) = 0 \qquad \forall \boldsymbol{\mu} \in \Lambda.$

In the previous problem, $\mathbf{X}^1$ can be computed, for instance, by assuming formally $\mathbf{X}^{-1} = 0$.

In the next proposition we prove an energy estimate similar to (15) when the potential energy density W is convex (see Assumption 1).

Proposition 3. *Let Assumption 1 hold and let $\mathbf{u}^n \in (H_0^1(\Omega))^d$ and $\mathbf{X}^n \in (H^1(\mathcal{B}))^d$ for $n = 0, \ldots, N$ satisfy Problem 3 with $\mathbf{X}^n \in (W^{1,\infty}(\mathcal{B}))^d$, then the following estimate holds true for all $n = 0, \ldots, N - 1$*

$$
\begin{aligned}
(17) \quad & \frac{\rho_f}{2\Delta t} \left(\|\mathbf{u}^{n+1}\|_0^2 - \|\mathbf{u}^n\|_0^2 \right) + \nu \| \boldsymbol{\nabla}_{\mathrm{sym}} \mathbf{u}^{n+1} \|_0^2 \\
& + \frac{\delta\rho}{2\Delta t} \left(\left\| \frac{\mathbf{X}^{n+1} - \mathbf{X}^n}{\Delta t} \right\|_{0,\mathcal{B}}^2 - \left\| \frac{\mathbf{X}^n - \mathbf{X}^{n-1}}{\Delta t} \right\|_{0,\mathcal{B}}^2 \right) + \frac{E(\mathbf{X}^{n+1}) - E(\mathbf{X}^n)}{\Delta t} \le 0
\end{aligned}
$$

Proof. Working similarly as in the continuous case, we take $\mathbf{v} = \mathbf{u}^{n+1}$ in (16a), using (16b) and the fact that $b(\mathbf{u}^n, \mathbf{u}^{n+1}, \mathbf{u}^{n+1}) = 0$ by definition, we have

$$
\rho_f \left(\frac{\mathbf{u}^{n+1} - \mathbf{u}^n}{\Delta t}, \mathbf{u}^{n+1} \right) + a(\mathbf{u}^{n+1}, \mathbf{u}^{n+1}) + \mathbf{c}_1(\boldsymbol{\lambda}^{n+1}, \mathbf{u}^{n+1}(\mathbf{X}^n)) = 0.
$$

The well-known identity $2(x - y)x = x^2 + (x - y)^2 - y^2$ and the definition of the bilinear form a imply

$$
(18) \quad \frac{\rho_f}{2\Delta t} \left(\|\mathbf{u}^{n+1}\|_0^2 - \|\mathbf{u}^n\|_0^2 \right) + \nu \| \boldsymbol{\nabla}_{\mathrm{sym}} \mathbf{u}^{n+1} \|_0^2 + \mathbf{c}_1(\boldsymbol{\lambda}^{n+1}, \mathbf{u}^{n+1}(\mathbf{X}^n)) \le 0.
$$

Let us now take $\mathbf{Y} = (\mathbf{X}^{n+1} - \mathbf{X}^n)/\Delta t$ in (16c) and recall that $\boldsymbol{\nabla}_s \mathbf{X} = \mathbb{F}$ so that

$$
\begin{aligned}
(19) \quad & \frac{\delta\rho}{\Delta t} \left(\frac{\mathbf{X}^{n+1} - \mathbf{X}^n}{\Delta t} - \frac{\mathbf{X}^n - \mathbf{X}^{n-1}}{\Delta t}, \frac{\mathbf{X}^{n+1} - \mathbf{X}^n}{\Delta t} \right)_{\mathcal{B}} \\
& + \left(\mathbb{P}(\mathbb{F}^{n+1}), \frac{\mathbb{F}^{n+1} - \mathbb{F}^n}{\Delta t} \right)_{\mathcal{B}} - \mathbf{c}_2 \left(\boldsymbol{\lambda}^{n+1}, \frac{\mathbf{X}^{n+1} - \mathbf{X}^n}{\Delta t} \right) = 0.
\end{aligned}
$$

Let us discuss in detail the second nonlinear term. We want to show its relation with the elastic potential energy (7). We define $\mathcal{W} : [0,1] \to \mathbb{R}$ as

$$
\mathcal{W}(t) := W(\mathbb{F}^n + t(\mathbb{F}^{n+1} - \mathbb{F}^n)),
$$

hence by chain rule we have thanks to (6)

$$
\mathcal{W}'(t) = \mathbb{P}(\mathbb{F}^n + t(\mathbb{F}^{n+1} - \mathbb{F}^n)) : (\mathbb{F}^{n+1} - \mathbb{F}^n).
$$

Thanks to Assumption 1, $\mathcal{W}$ is convex, therefore we have that $\mathcal{W}'(1) \ge \mathcal{W}(1) - \mathcal{W}(0)$ from which we obtain

$$
\begin{aligned}
\left(\mathbb{P}(\mathbb{F}^{n+1}), \frac{\mathbb{F}^{n+1} - \mathbb{F}^n}{\Delta t} \right)_{\mathcal{B}} &= \frac{1}{\Delta t} \int_{\mathcal{B}} \mathcal{W}'(1) \mathrm{d}\mathbf{s} \\
&\ge \frac{1}{\Delta t} \int_{\mathcal{B}} (\mathcal{W}(1) - \mathcal{W}(0)) \mathrm{d}\mathbf{s} = \frac{1}{\Delta t} (E(\mathbf{X}^{n+1}) - E(\mathbf{X}^n)).
\end{aligned}
$$

Inserting the last inequality in (19) with standard computations, we arrive at

$$
\begin{aligned}
(20) \quad & \frac{\delta\rho}{2\Delta t} \left(\left\| \frac{\mathbf{X}^{n+1} - \mathbf{X}^n}{\Delta t} \right\|_{0,\mathcal{B}}^2 - \left\| \frac{\mathbf{X}^n - \mathbf{X}^{n-1}}{\Delta t} \right\|_{0,\mathcal{B}}^2 \right) \\
& + \frac{1}{\Delta t} (E(\mathbf{X}^{n+1}) - E(\mathbf{X}^n)) - \mathbf{c}_2 \left(\boldsymbol{\lambda}^{n+1}, \frac{\mathbf{X}^{n+1} - \mathbf{X}^n}{\Delta t} \right) \le 0.
\end{aligned}
$$

Summing up (18) and (20) and taking into account (16d), we arrive at (17). $\qquad \square$

We observe that the energy estimate reported in Proposition 3 does not require any limitation on the time step.

5. Finite element discretization

In this section we introduce the finite element discretization of Problem 3. For this we consider a family $\mathcal{T}_h$ of regular meshes in Ω and a family $\mathcal{S}_h$ of regular meshes in $\mathcal{B}$. We denote by h_x and h_s the meshsize of $\mathcal{T}_h$ and $\mathcal{S}_h$, respectively. Let $V_h \subseteq (H_0^1(\Omega))^d$ and $Q_h \subseteq L_0^2(\Omega)$ be finite element spaces which satisfy the usual discrete ellipticity on the kernel and the discrete inf-sup conditions for the Stokes problem [2]. Moreover, we consider finite dimensional subspaces $S_h \subseteq (H^1(\mathcal{B}))^d$ and $\Lambda_h \subseteq \Lambda$. Then the finite element counterpart of Problem 3 reads.

Problem 4. *Given* $\mathbf{u}_{0h} \in V_h$ *and* $\mathbf{X}_0 \in W^{1,\infty}(\mathcal{B})$, *for* $n = 1, \ldots, N$ *find* $\mathbf{u}_h^n, p_h^n \in V_h \times Q_h$, $\mathbf{X}_h^n \in S_h$, *and* $\boldsymbol{\lambda}_h^n \in \Lambda_h$, *such that*

$$\rho_f \left(\frac{\mathbf{u}_h^{n+1} - \mathbf{u}_h^n}{\Delta t}, \mathbf{v} \right) + b(\mathbf{u}_h^n, \mathbf{u}_h^{n+1}, v) + a(\mathbf{u}_h^{n+1}, \mathbf{v})$$

$$\text{(21a)} \qquad - (\operatorname{div} \mathbf{v}, p_h^{n+1}) + \mathbf{c}_1(\boldsymbol{\lambda}_h^{n+1}, v(\mathbf{X}_h^n)) = 0 \qquad \forall \mathbf{v} \in V_h$$

$$\text{(21b)} \qquad (\operatorname{div} \mathbf{u}_h^{n+1}, q) = 0 \qquad \forall q \in Q_h$$

$$\delta\rho \left(\frac{\mathbf{X}_h^{n+1} - 2\mathbf{X}_h^n + \mathbf{X}_h^{n-1}}{\Delta t^2}, \mathbf{Y} \right)_{\mathcal{B}} + (\mathbb{P}(\mathbb{F}_h^{n+1}), \boldsymbol{\nabla}_s \mathbf{Y})_{\mathcal{B}}$$

$$\text{(21c)} \qquad - \mathbf{c}_2(\boldsymbol{\lambda}_h^{n+1}, \mathbf{Y}) = 0 \qquad \forall \mathbf{Y} \in S_h$$

$$\text{(21d)} \qquad \mathbf{c}_1(\boldsymbol{\mu}, \mathbf{u}_h^{n+1}(\mathbf{X}_h^n)) - \mathbf{c}_2 \left(\boldsymbol{\mu}, \frac{\mathbf{X}_h^{n+1} - \mathbf{X}_h^n}{\Delta t} \right) = 0 \qquad \forall \boldsymbol{\mu} \in \Lambda_h.$$

where $\mathbb{F}_h^{n+1} = \boldsymbol{\nabla}_s \mathbf{X}_h^{n+1}$.

With the same proof of Proposition 3, it can be shown that the solution $\mathbf{u}_h^n \in V_h$ and $\mathbf{X}_h^n \in S_h$ satisfies an energy estimate analogous to (17).

Proposition 4. *Let Assumption 1 hold and let* $u_h^n \in V_h$ *and* $\mathbf{X}_h^n \in S_h$ *for* $n = 0, \ldots, N$ *satisfy Problem 4. Then the following estimate holds true for all* $n = 0, \ldots, N - 1$

$$\frac{\rho_f}{2\Delta t} \left(\|\mathbf{u}_h^{n+1}\|_0^2 - \|\mathbf{u}_h^n\|_0^2 \right) + \boldsymbol{\mu}\| \boldsymbol{\nabla}_{\mathrm{sym}} \mathbf{u}_h^{n+1}\|_0^2$$

$$\text{(22)} \qquad + \frac{\delta\rho}{2\Delta t} \left(\left\| \frac{\mathbf{X}_h^{n+1} - \mathbf{X}_h^n}{\Delta t} \right\|_{0,\mathcal{B}}^2 - \left\| \frac{\mathbf{X}_h^n - \mathbf{X}_h^{n-1}}{\Delta t} \right\|_{0,\mathcal{B}}^2 \right) + \frac{E(\mathbf{X}_h^{n+1}) - E(\mathbf{X}_h^n)}{\Delta t} \leq 0.$$

In the next section we shall present some numerical results obtained using the scheme given by (21a)–(21d) where the term related to the Piola–Kirchhoff tensor is linear. From now on, $\mathbb{P}(\mathbb{F})$ will be defined as follows

$$\text{(23)} \qquad \mathbb{P}(\mathbb{F}) = \kappa\mathbb{F} = \kappa \boldsymbol{\nabla}_s \mathbf{X},$$

so that Problem 4 can be written in matrix form as follows:

$$\text{(24)} \qquad \begin{pmatrix} \mathsf{A} & \mathsf{B}^\top & 0 & \mathsf{L}_f(\mathbf{X}_h^n)^\top \\ \mathsf{B} & 0 & 0 & 0 \\ \hline 0 & 0 & \mathsf{A}_s & -\mathsf{L}_s^\top \\ \mathsf{L}_f(\mathbf{X}_h^n) & 0 & -\mathsf{L}_s & 0 \end{pmatrix} \begin{pmatrix} \mathbf{u}_h^{n+1} \\ p_h^{n+1} \\ \hline \mathbf{X}_h^{n+1} \\ \boldsymbol{\lambda}_h^{n+1} \end{pmatrix} = \begin{pmatrix} \mathsf{f} \\ 0 \\ \hline \mathsf{g} \\ \mathsf{d} \end{pmatrix}$$

where, denoting by φ, ψ, χ and ζ the basis functions respectively in V_h, Q_h, S_h and Λ_h, we have used the following notation:

$$\mathsf{A} = \frac{\rho_f}{\Delta t}\mathsf{M}_f + \mathsf{K}_f \quad \text{with } (\mathsf{M}_f)_{ij} = (\varphi_j, \varphi_i), \ (\mathsf{K}_f)_{ij} = a(\varphi_j, \varphi_i) + b(\mathbf{u}_h^n, \varphi_j, \varphi_i)$$
$$\mathsf{B}_{ki} = -(\operatorname{div}\varphi_i, \psi_k)$$
$$\mathsf{A}_s = \frac{\delta\rho}{\Delta t^2}\mathsf{M}_s + \mathsf{K}_s \quad \text{with } (\mathsf{M}_s)_{ij} = (\chi_j, \chi_i)_{\mathcal{B}}, \ (\mathsf{K}_s)_{ij} = \kappa(\boldsymbol{\nabla}_s\chi_j, \boldsymbol{\nabla}_s\chi_i)_{\mathcal{B}}$$
$$(\mathsf{L}_f(\mathbf{X}_h^n))_{lj} = \mathbf{c}_1(\zeta_l, \varphi_j(\mathbf{X}_h^n))$$
$$(\mathsf{L}_s)_{lj} = \mathbf{c}_2(\zeta_l, \chi_j)$$
$$\mathsf{f}_i = \frac{\rho_f}{\Delta t}(\mathsf{M}_f\mathbf{u}_h^n)_i$$
$$\mathsf{g}_i = \frac{\delta\rho}{\Delta t^2}\left(\mathsf{M}_s(2\mathbf{X}_h^n - \mathbf{X}_h^{n-1})\right)_i$$
$$\mathsf{d}_l = -\frac{1}{\Delta t}(\mathsf{L}_s\mathbf{X}_h^n)_l.$$

6. Numerical Experiments

In this section we perform a wide set of tests that numerically explore the scheme characteristics. In all simulations reported in this section the velocity and pressure spaces are discretized using the enhanced Bercovier–Pironneau element introduced in [3], that is $P_1\text{iso}\,P_2/(P_1 + P_0)$ element. For $k > 0$, P_k stands for the space of continuous piecewise polynomials of degree not greater than k and P_0 is the space of piecewise constants. Performances of the DLM-IBM scheme will be compared to the classical pointwise FE-IBM.

In order to make the presentation clearer, let us recall the FE-IBM scheme when the Piola–Kirchhoff tensor is defined as in (23).

For $n = 0, \ldots, N - 1$ we perform the following three steps.

Step 1: Compute the *fluid-structure interaction* force vector F^{n+1} as

$$\mathsf{F}_i^{n+1} = -\kappa(\boldsymbol{\nabla}_s\mathbf{X}_h^n, \varphi_i(\mathbf{X}_h^n))_{\mathcal{B}}$$

Step 2: Solve the Navier–Stokes equations

$$\begin{pmatrix} \mathsf{A} + \frac{\delta\rho}{\Delta t}\mathsf{M}_{\mathcal{B}} & \mathsf{B}^\top \\ \mathsf{B} & 0 \end{pmatrix}\begin{pmatrix} \mathbf{u}_h^{n+1} \\ p_h^{n+1} \end{pmatrix} = \begin{pmatrix} \mathsf{f} + \mathsf{F}^{n+1} + \frac{\delta\rho}{\Delta t}\mathsf{M}_{\mathcal{B}}\mathbf{u}_h^n \\ 0 \end{pmatrix}.$$

Here $(\mathsf{M}_{\mathcal{B}})_{ij} = (\varphi_j(\mathbf{X}_h^n), \varphi_i(\mathbf{X}_h^n))_{\mathcal{B}}$.

Step 3: Update pointwise the structure position. For M structure points, compute for the i-th point position:

(25)
$$\frac{\mathbf{X}_{hi}^{n+1} - \mathbf{X}_{hi}^n}{\Delta t} = \mathbf{u}_h^{n+1}(\mathbf{X}_{hi}^n) \quad \forall i = 1, \ldots, M.$$

The first goal of our numerical experiments is to confirm the better behavior of DLM-IBM with respect to FE-IBM for what the CFL condition is concerned. To this aim, we start recalling the CFL condition that has been proved in [5]. In two space dimensions, when the solid has codimension one, the time step Δt should be smaller than a multiple of $h_x h_s$, while when the solid has codimension zero, then Δt has to be bounded by a multiple of h_x. On the other hand, in Proposition 3 we

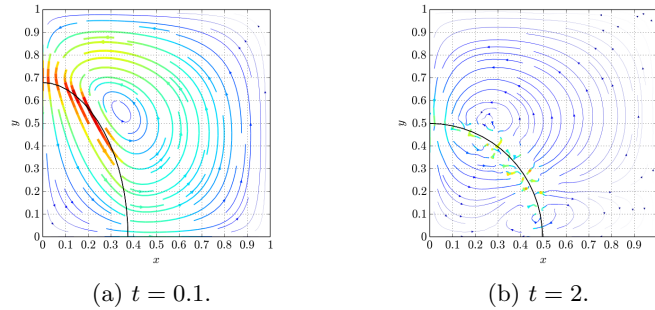(a) $t = 0.1$.   (b) $t = 2$.

FIGURE 1. Codimension one structure position snapshots. The pictures represent the velocity streamlines and the structure position for the first and final time steps. The streamline color pictures the velocity magnitude, red is the higher value.
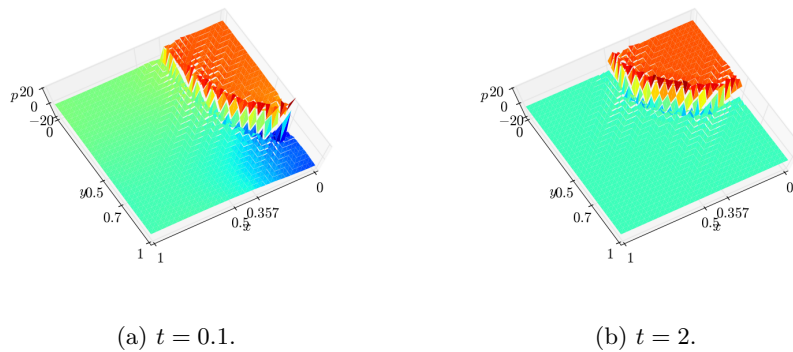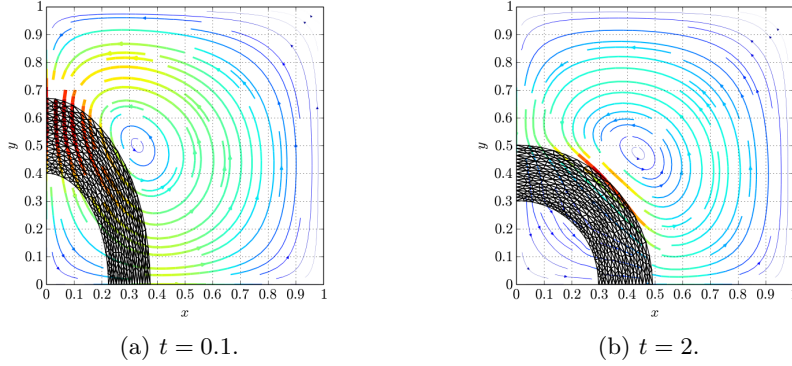

(a) $t = 0.1$.   (b) $t = 2$.

FIGURE 2. Codimension one pressure snapshots. The pictures represent the resulting pressure map for the first and final time steps.

proved that the DLM-IBM is unconditionally stable, that is no restriction on Δt is required for its stability.

A series of tests will be performed, using the classical benchmark problem of an ellipsoidal structure that evolves to a circular equilibrium position. The ellipsoid is centered at the midpoint of our (square) physical domain and the initial fluid is at rest, so that we can reduce the computational domain to a quarter of the physical one by symmetry conditions. Figure 1 reports the initial and final configurations of our test (codimension one) as a result of a computation performed with DLM-IBM. The corresponding pressure is plotted in Figure 2. Analogue plots are reported in Figures 3 and 4, respectively, in the case of codimension zero structure. The x and y thicks on the pressure plot correspond to the initial and final position of the structure.

(a) $t = 0.1$.

(b) $t = 2$.

FIGURE 3. Codimension zero structure position snapshots. The pictures represent the velocity streamlines and the structure position for the first and final time steps. The streamline color pictures the velocity magnitude, red is the higher value.
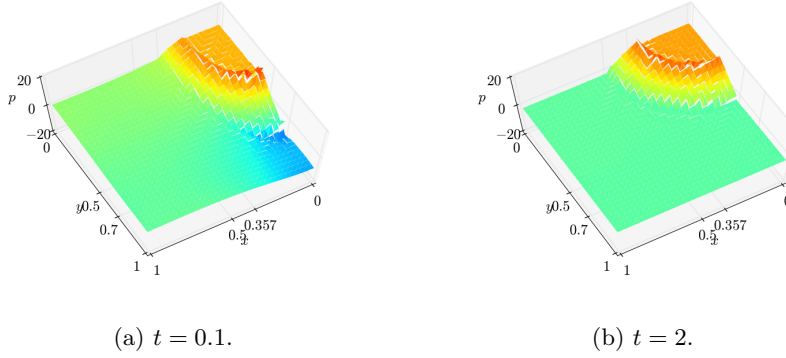

(a) $t = 0.1$.

(b) $t = 2$.

FIGURE 4. Codimension zero pressure snapshots. The pictures represent the resulting pressure map for the first and final time steps.

In order to check the stability with respect to the time step, we consider the fluid and structure kinematic and elastic energy:

$$(26) \qquad \Pi(\mathbf{X}_h^n, \mathbf{u}_h^n) = \frac{\rho_f}{2}\|\mathbf{u}_h^n\|_0^2 + \frac{\delta\rho}{2}\left\|\frac{\mathbf{X}_h^n - \mathbf{X}_h^{n-1}}{\Delta t}\right\|_{0,\mathcal{B}}^2 + E(\mathbf{X}_h^n).$$

We compute the energy ratio: $\Pi(\mathbf{X}_h^n, \mathbf{u}_h^n)/\Pi(\mathbf{X}_h^0, \mathbf{u}_h^0)$ for different parameter definitions as a function of time for both FE-IBM and DLM-IBM computations. Figures 5 and 6 show the results in the case of the codimension one structure when $\delta\rho = 0$ and $\delta\rho = 0.3$, respectively. Figure 7 reports on the case of codimension zero structure when $\delta\rho = 0.3$.

(a) $\Delta t = 10^{-1}$, $h_s = 1/8$. (b) $\Delta t = 10^{-1}$, $h_s = 1/16$. (c) $\Delta t = 10^{-1}$, $h_s = 1/32$.

(d) $\Delta t = 5 \cdot 10^{-2}$, $h_s = 1/8$. (e) $\Delta t = 5 \cdot 10^{-2}$, $h_s = 1/16$. (f) $\Delta t = 5 \cdot 10^{-2}$, $h_s = 1/32$.
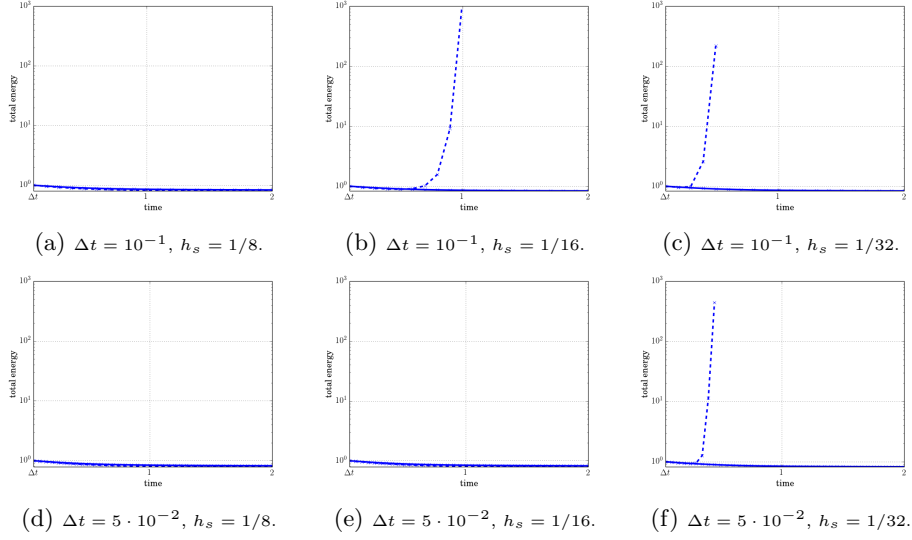
FIGURE 5. Energy ratio for codimension one structure. The structure elastic constant $\kappa = 5$, $h_x = 1/32$, the fluid viscosity $\nu = 1$, $\delta\rho = 0$. The solid line correspond to the DLM-IBM scheme, while the dashed line marks the energy for the FE-IBM scheme.

More precisely, Figures 5 and 6 show the energy ratio for a fixed $h_x = 1/32$, and varying h_s (row-wise) and Δt (column-wise). It is clear that the FE-IBM (dashed curve) has a blowing-up energy if h_s is too small compared to Δt.

Figure 7 shows the energy ratio for a fixed $h_s = 1/8$, and varying h_x (row-wise) and Δt (column-wise). It can be seen that the energy computed with the FE-IBM (dashed curve) blows up if Δt is not small enough with respect to h_x.

On the other hand, in all cases it can be appreciated that the DLM-IBM does not need any constraint on Δt in order to be stable,

Since the fluid considered in our experiments is incompressible, an important physical property that has to be preserved is the mass conservation of the coupled scheme (see [3, 4] for related work in this framework). It turns out that, unexpectedly, the DLM-IBM scheme enjoys better conservation properties than the FE-IBM. We do not have a theoretical explanation for this phenomenon yet; in Figure 8 we report the comparison between the two cases (structure of codimension one). In Figures 8(a) and 8(b) we report the evolution of the structure position during the simulation. Here it is already clear how better is the mass preservation for the DLM-IBM scheme. To make this result even clearer, in Figure 8(c) we present the final structure position for both schemes.

This phenomenon is more evident when higher order schemes are used. For instance, in Figure 9 we show the results of the same simulation when the enhanced Hood–Taylor Stokes element $P_3 - (P_2^c + P_1)$ is used. The justification of this effect is currently under investigation.

We conclude this section with some algorithmic comments which might be useful in order to have a more accurate solution. The solution of system (24) can be interpreted as a semi-implicit discretization of the original fluid-structure problem.
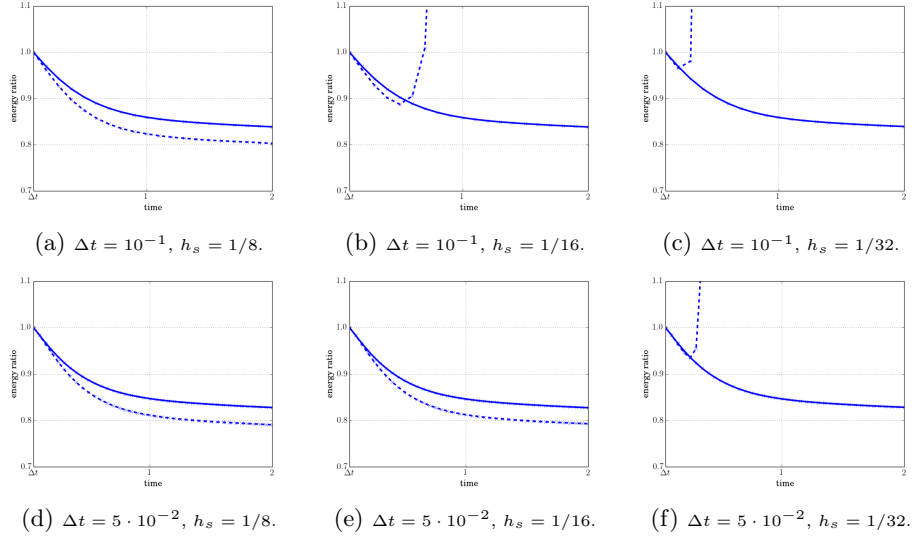
FIGURE 6. Energy ratio for codimension one structure. The structure elastic constant $\kappa = 5$, $h_x = 1/32$, the fluid viscosity $\nu = 1$, $\delta\rho = 0.3$. The solid line correspond to the DLM-IBM scheme, while the dashed line marks the energy for the FE-IBM scheme.
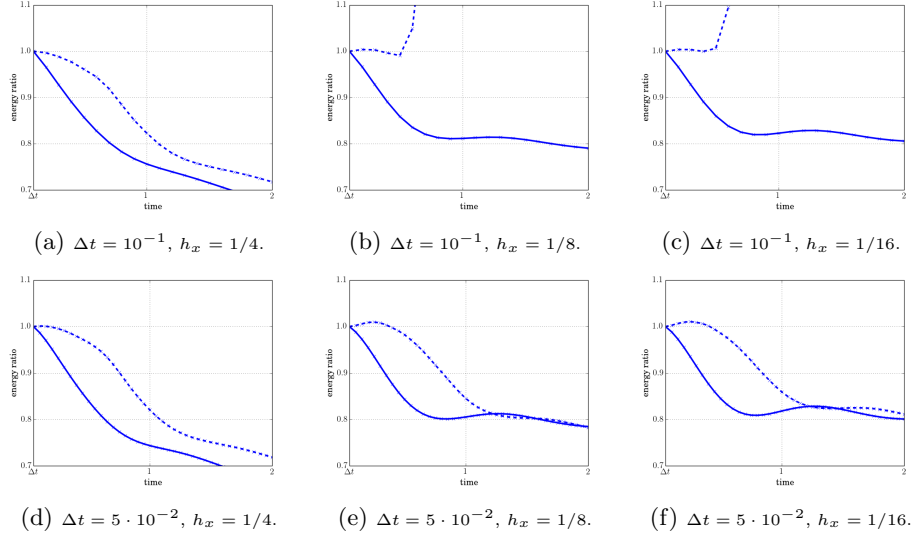
(a) $\Delta t = 10^{-1}$, $h_s = 1/8$.

(b) $\Delta t = 10^{-1}$, $h_s = 1/16$.

(c) $\Delta t = 10^{-1}$, $h_s = 1/32$.

(d) $\Delta t = 5 \cdot 10^{-2}$, $h_s = 1/8$.

(e) $\Delta t = 5 \cdot 10^{-2}$, $h_s = 1/16$.

(f) $\Delta t = 5 \cdot 10^{-2}$, $h_s = 1/32$.

FIGURE 7. Energy ratio for codimension zero structure. The structure elastic constant $\kappa = 1$, $h_s = 1/8$, the fluid viscosity $\nu = 0.05$, $\delta\rho = 0.3$. The solid line correspond to the DLM-IBM scheme, while the dashed line marks the energy for the FE-IBM scheme.

(a) $\Delta t = 10^{-1}$, $h_x = 1/4$.

(b) $\Delta t = 10^{-1}$, $h_x = 1/8$.

(c) $\Delta t = 10^{-1}$, $h_x = 1/16$.

(d) $\Delta t = 5 \cdot 10^{-2}$, $h_x = 1/4$.

(e) $\Delta t = 5 \cdot 10^{-2}$, $h_x = 1/8$.

(f) $\Delta t = 5 \cdot 10^{-2}$, $h_x = 1/16$.

(a) DLM-IBM.

(b) FE-IBM.

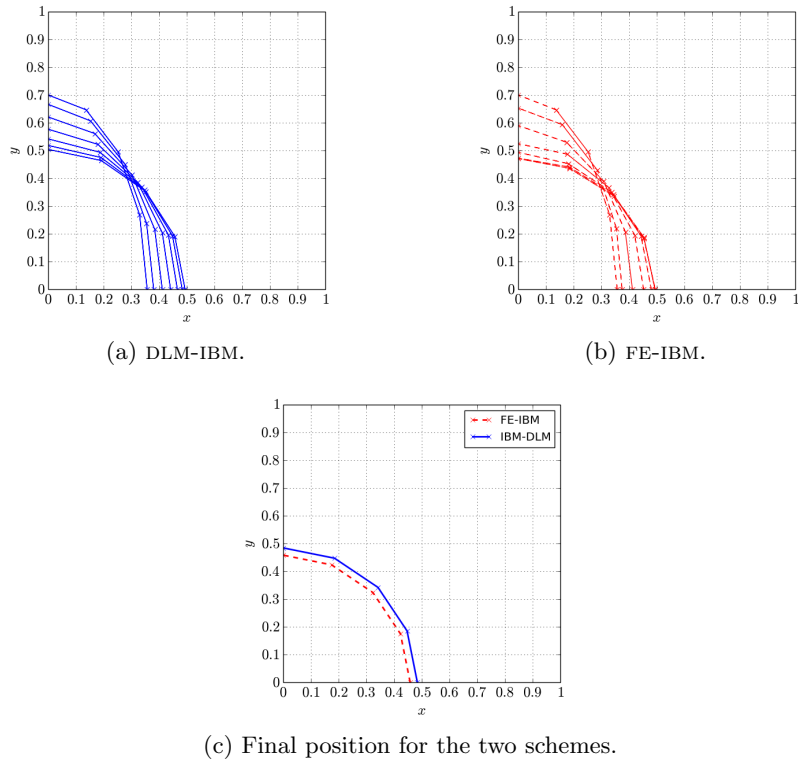(c) Final position for the two schemes.

FIGURE 8. Comparison of mass conservation for the DLM-IBM (left) and FE-IBM (right) schemes
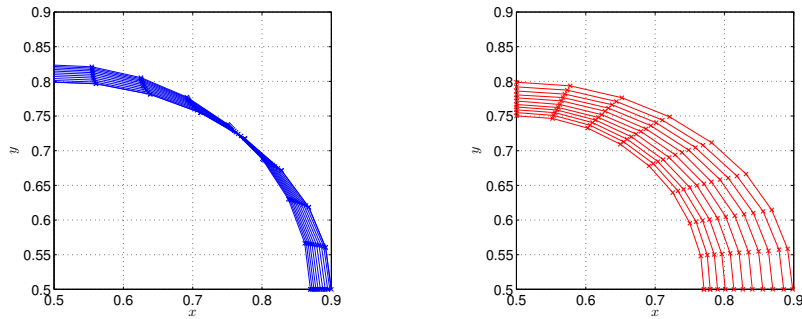

FIGURE 9. Mass conservation of the DLM-IBM (left) and FE-IBM (right) with higher order fluid element.

The strategy we are going to describe represents a first investigation towards the approximation of a fully implicit scheme.

The resulting algorithm (based on a fixed point iteration) is pretty simple: in the following the discretization index h will be omitted for the sake of clearness. Consider the n-th time step and the k-th iteration and denote $\mathbf{X}_0 = \mathbf{X}^n$. For $k \geq 1$

we solve:

$$
\begin{pmatrix}
\mathsf{A} & \mathsf{B}^\top & 0 & \mathsf{L}_f(\mathbf{X}_{k-1})^\top \\
\mathsf{B} & 0 & 0 & 0 \\
\hline
0 & 0 & \mathsf{A}_s & -\mathsf{L}_s^\top \\
\mathsf{L}_f(\mathbf{X}_{k-1}) & 0 & -\mathsf{L}_s & 0
\end{pmatrix}
\begin{pmatrix}
\mathbf{u}_k \\
p_k \\
\hline
\mathbf{X}_k \\
\boldsymbol{\lambda}_k
\end{pmatrix}
=
\begin{pmatrix}
\mathsf{f} \\
0 \\
\hline
\mathsf{g} \\
\mathsf{d}
\end{pmatrix}.
$$

We consider the fluid-structure coupling residual as

$$
(27) \qquad r\left(\mathbf{u}_k, \mathbf{X}_k\right) = \left\| \mathsf{L}_f(\mathbf{X}_k)\mathbf{u}_k - \frac{\mathsf{L}_s\mathbf{X}_k - \mathsf{L}_s\mathbf{X}^n}{\Delta t} \right\|_{0,\mathcal{B}}.
$$

If $r\left(\mathbf{u}_k, \mathbf{X}_k\right) \le \varepsilon$ we set $(\mathbf{u}^{n+1}, p^{n+1}, \boldsymbol{\lambda}^{n+1}, \mathbf{X}^{n+1}) = (\mathbf{u}_k, p_k, \boldsymbol{\lambda}_k, \mathbf{X}_k)$, otherwise continue iterating. The residual values for ten iterations, (corresponding to ten consecutive time steps) are represented in Figure 10. Both codimension one and zero are considered. The simulation parameters are specified in the figure caption. Different lines correspond to different time steps (generally, the top lines correspond to the first time step, and so on monotonically down to the bottom line corresponding to the tenth time step). It is interesting to notice that the residual decreases as the structure approaches a stationary state. Moreover, and most importantly, within the same time step, the algorithm converges with approximately first order. This property is important in view of designing multigrid type algorithms in order to reduce the computational cost of the implicit scheme.

Finally, in Figure 11 we present some snapshots of the simulation of a codimension zero solid which is a square at its equilibrium configuration. In the initial configuration the solid is stretched and has a rectangular shape. At the beginning of the simulation, Figure 11(a), the corner of the structure imposes a singularity to velocity field and a vortex arises. In snapshot 11(b) the structure is bouncing along the x axis. In Figure 11(c) the structure interacts again with the fluid, as it is heading to the equilibrium position, a second vortex arises as a consequence of the structure motion. In Figure 11(d) the structure has almost approached its equilibrium position.

7. Conclusions

In this paper we presented a new formulation for the finite element approximation of fluid-structure interaction problems within the setting of the Immersed Boundary Method. With this formulation the coupling between the fluid and the structure is modeled with the help of a distributed Lagrange multiplier, so that a fully variational problem is obtained. The main feature of the fully discrete scheme associated with this formulation, is that its stability does not require any restriction on the time step size.

Numerical experiments confirm the theoretical energy estimates.

References

[1] F. Auricchio, D. Boffi, L. Gastaldi, A. Lefieux, and A. Reali. On a fictitious domain method with distributed Lagrange multiplier for interface problems. *Applied Numerical Mathematics*, 2014. To appear.

[2] D. Boffi, F. Brezzi, and M. Fortin. *Mixed Finite Element Methods and Applications*, volume 44 of *Springer Series in Computational Mathematics*. Springer-Verlag, New York, 2013.

[3] D. Boffi, N. Cavallini, F. Gardini, and L. Gastaldi. Local mass conservation of Stokes finite elements. *J. Sci. Comput.*, 52(2):383–400, 2012.
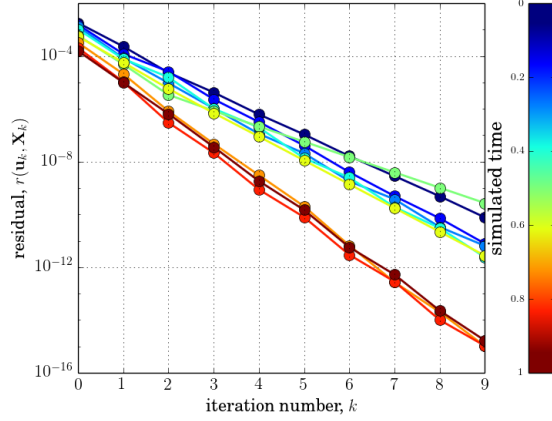
(a) Codimension one.
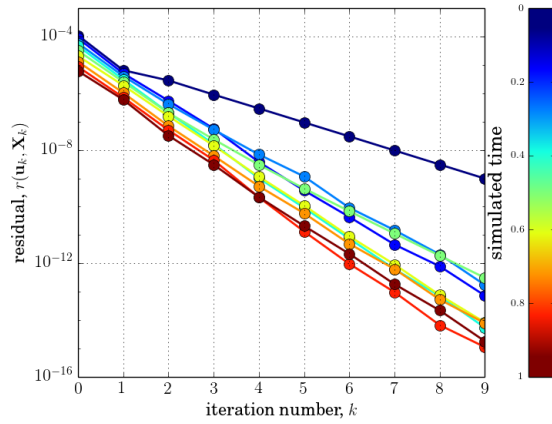
(b) Codimension zero.

FIGURE 10. Convergence for fixed point iteration for the fluid-structure interaction nonlinear coupling. The simulation parameters are $h_x = h_s = 1/8$, $\kappa = 8$, $\Delta t = 1/10$, results are presented for codimension one and zero. The residual is defined in equation (27). Different color refer to different simulated times.

[4] D. Boffi, N. Cavallini, F. Gardini, and L. Gastaldi. Stabilized Stokes elements and local mass conservation. *Boll. Unione Mat. Ital. (9)*, 5(3):543–573, 2012.

[5] D. Boffi, N. Cavallini, and L. Gastaldi. Finite element approach to immersed boundary method with different fluid and solid densities. *Math. Models Methods Appl. Sci.*, 21(12):2523–2550, 2011.

[6] D. Boffi and L. Gastaldi. A finite element approach for the immersed boundary method. *Comput. & Structures*, 81(8-11):491–501, 2003. In honour of Klaus-Jürgen Bathe.

[7] D. Boffi, L. Gastaldi, and L. Heltai. Numerical stability of the finite element immersed boundary method. *Math. Models Methods Appl. Sci.*, 17(10):1479–1505, 2007.

[8] D. Boffi, L. Gastaldi, and L. Heltai. On the CFL condition for the finite element immersed boundary method. *Comput. & Structures*, 85(11-14):775–783, 2007.

(a) $t = 0.03$.   (b) $t = 0.17$.
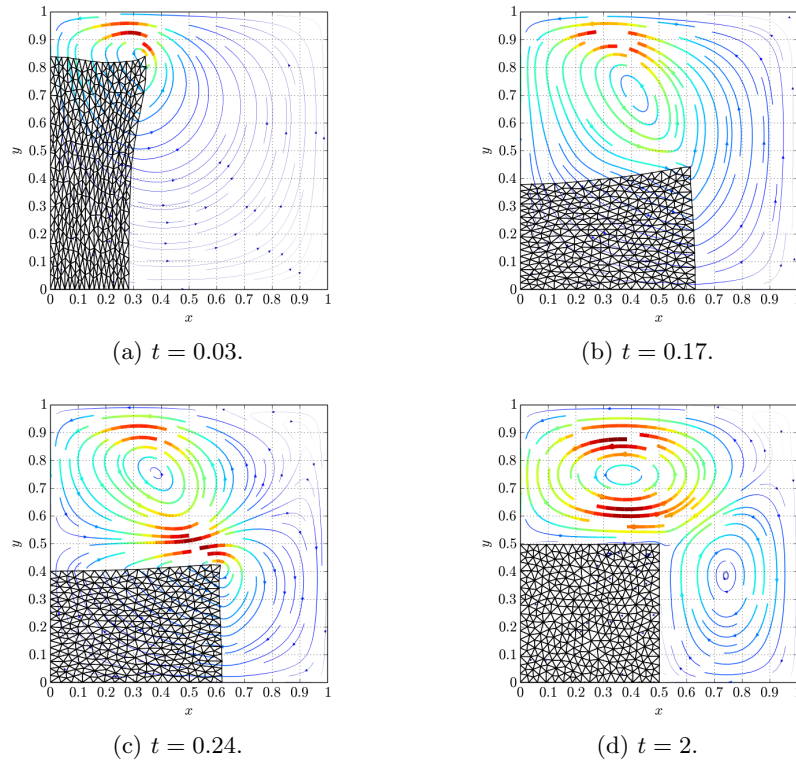
(c) $t = 0.24$.   (d) $t = 2$.

FIGURE 11. Simulation of a square structure that moves from an initial rectangular position to the equilibrium position. The fluid mesh $h_x = 1/32$, the structure one is $h_s = 1/16$, $\Delta t = 10^{-3}$. The fluid viscosity is $\nu = 0.01$ and the structure elastic constant is 100.

[9] D. Boffi, L. Gastaldi, L. Heltai, and C. S. Peskin. On the hyper-elastic formulation of the immersed boundary method. *Comput. Methods Appl. Mech. Engrg.*, 197(25-28):2210–2231, 2008.

[10] D. Boffi, L. Gastaldi, and M. Ruggeri. Mixed formulation for interface problems with distributed Lagrange multiplier. Submitted, 2014.

[11] P. Causin, J. F. Gerbeau, and F. Nobile. Added-mass effect in the design of partitioned algorithms for fluid-structure problems. *Comput. Methods Appl. Mech. Engrg.*, 194(42-44):4506–4527, 2005.

[12] V. Girault and R. Glowinski. Error analysis of a fictitious domain method applied to a Dirichlet problem. *Japan J. Indust. Appl. Math.*, 12(3):487–514, 1995.

[13] V. Girault, R. Glowinski, and T. W. Pan. A fictitious-domain method with distributed multiplier for the Stokes problem. In *Applied nonlinear analysis*, pages 159–174. Kluwer/Plenum, New York, 1999.

[14] R. Glowinski and Yu. Kuznetsov. Distributed Lagrange multipliers based on fictitious domain method for second order elliptic problems. *Comput. Methods Appl. Mech. Engrg.*, 196(8):1498–1506, 2007.

[15] L. Heltai. On the stability of the finite element immersed boundary method. *Comput. & Structures*, 86(7-8):598–617, 2008.

[16] L. Heltai and F. Costanzo. Variational implementation of immersed finite element methods. *Comput. Methods Appl. Mech. Engrg.*, 229/232:110–127, 2012.

[17] W. K. Liu, D. W. Kim, and S. Tang. Mathematical foundations of the immersed finite element method. *Comput. Mech.*, 39(3):211–222, 2007.
[18] C. S. Peskin. The immersed boundary method. *Acta Numer.*, 11:479–517, 2002.
[19] X. Wang and W.K. Liu. Extended immersed boundary method using FEM and RKPM. *Comput. Methods Appl. Mech. Engrg.*, 193:1305–1321, 2004.
[20] L. Zhang, A. Gerstenberger, X. Wang, and W.K. Liu. Immersed finite element method. *Comput. Methods Appl. Mech. Engrg.*, 193:2051–2067, 2004.

DIPARTIMENTO DI MATEMATICA "F. CASORATI", UNIVERSITÀ DI PAVIA, ITALY
E-mail address: daniele.boffi@unipv.it
URL: http://www-dimat.unipv.it/boffi/

DIPARTIMENTO DI MATEMATICA "F. CASORATI", UNIVERSITÀ DI PAVIA, ITALY
E-mail address: nicola.cavallini@unipv.it
URL: http://www-dimat.unipv.it/~cavallini/

DICATAM, UNIVERSITÀ DI BRESCIA, ITALY
E-mail address: lucia.gastaldi@unibs.it
URL: http://www.ing.unibs.it/gastaldi/